Bull Volcanol (1999) 60:595–609

ORIGINAL PAPER

M. Polacci · K. V. Cashman · J. P. Kauahikaua

Textural characterization of the pāhoehoe–ʻaʻā transition in Hawaiian basalt

Received: 15 May 1998 / Accepted: 21 October 1998

Abstract Pāhoehoe and ʻaʻā are the most common surface morphologies in basaltic lava flows, yet no predictive models exist to link physical parameters of flow emplacement to changes in their surface textures and rheological properties. We have characterized changes of vesicularity, vesicle deformation, and crystallinity across the pāhoehoe–ʻaʻā transition as preserved in two different eruptions, a brief, high-velocity effusion of lava from Kīlauea Volcano on 1 February 1996, and a small breakout from an ephemeral vent within a larger channel produced during the 1868 eruption of Mauna Loa. This allowed us to compare conditions leading to the pāhoehoe–ʻaʻā transition for both open channel flow (Kīlauea 1996) and reactivation of lava from an ephemeral vent (Mauna Loa 1868). Textural changes across the transition include (a) decrease in vesicularity and vesicle number density, (b) increase in microlite crystallinity and crystal number density, and (c) increase in vesicle deformation. The results support past qualitative descriptions of the transition and highlight the importance of plagioclase crystallinity in controlling lava rheology and surface morphology.

Key words Hawaiian basalt · Pāhoehoe–ʻaʻā transition · Textural characterization

Editorial responsibility: M. Carroll

M. Polacci (✉)
Dipartimento di Scienze della Terra, via S. Maria 53,
I-56126 Pisa, Italy
e-mail: polacci@dst.unipi.it

K. V. Cashman
Department of Geological Sciences, University of Oregon,
Eugene, OR 97403–1272, USA

J. P. Kauahikaua
USGS, Hawaiian Volcano Observatory, Hawaii National Park,
Hawaii 96718, USA

Introduction

Vesiculation processes drive the dynamics of basaltic eruptions and control the style of basaltic lava emplacement. Rates and amounts of volatile release control the heights of lava fountains (Wilson and Head 1981; Head and Wilson 1987), transitions between explosive and effusive eruptive behavior (Parfitt and Wilson 1995), and the degree to which crystallization occurs in response to degassing (Sparks and Pinkerton 1978; Lipman et al. 1985; Lipman and Banks 1987; Crisp et al. 1994). Less well understood are the details of degassing and crystallization after eruption and how lava transport styles are coupled to gas and heat loss through rheological changes produced by bubble deformation and lava crystallization (Dragoni 1993; Crisp et al. 1994).

Pāhoehoe and ʻaʻā lava flows differ superficially in surface texture but fundamentally in emplacement mechanism. Here we study the morphologic transformation of crust-dominated pāhoehoe lava to core-dominated ʻaʻā lava to constrain the relative timing of crust rupture, lava cooling, and crystallization, processes that irreversibly transform pāhoehoe to ʻaʻā lava. We address this problem through a study of textural changes preserved across the pāhoehoe–ʻaʻā transition in two lava flows, one emplaced at Kīlauea Volcano on 1 February 1996, and the other during the 1868 eruption of Mauna Loa Volcano. In both, the transition is preserved over several meters and glass (melt quenched so that original crystallization textures are preserved) is preserved at the upper flow surface. We document changes in both vesicle and crystal populations across the transition. Changes in crystal content can be related to lava temperatures and cooling rates, whereas vesicle shapes can preserve information on strain rates. These small-scale changes, in turn, can be related to observed (e.g., Peterson and Tilling 1980; Kilburn 1981, 1990; Kilburn and Guest 1993) changes in lava flow behavior.

Pāhoehoe and ‘a‘ā

Pāhoehoe and ‘a‘ā have contrasting surface morphologies (smooth and rough, respectively). Decades of field observations have shown that they reflect fundamentally different conditions of lava transport and emplacement (e.g., Macdonald 1953, 1967, 1972; Pinkerton and Sparks 1976; Peterson and Tilling 1980; Kilburn 1981, 1990, 1993; Chester et al. 1985; Rowland and Walker 1987, 1990) and produce flow fields of different shapes and dimensions. Pāhoehoe flows advance slowly enough that rapidly formed surface crusts are preserved, and conditions of emplacement are thus dictated by the balance between crustal strength and lava flux (e.g., Fink and Griffiths 1990; Hon et al. 1994). Heat loss from lava is limited (Cashman et al. 1994; Keszthelyi 1994, 1995), so that downflow crystallization is minor except when lava is stored locally (e.g., in tumuli) prior to reactivation. These flows are considered to be crust-dominated in their behavior (Kilburn 1993). In contrast, ‘a‘ā flow advance is sufficiently rapid that the tensile strength of the lava crust is overcome by the imposed stress, and flow crusts are continuously disrupted. Flow advance is controlled by the rheology of the lava core (Kilburn 1993). Heat loss, dominated by radiative cooling from the continuously exposed flow core in the upper parts of the channel (Crisp and Baloga 1990, 1994), is high and leads to early high rates of crystallization (Cashman et al. 1997). As a consequence, lava crystallinity increases dramatically downflow (Crisp et al. 1994). Increasing crystallinity, in turn, changes flow rheology by increasing lava viscosity and introducing non-Newtonian effects (both a yield strength and a strain-dependent viscosity (Dingwell and Webb 1989; Webb and Dingwell 1990; Pinkerton and Stevenson 1992; Crisp et al. 1994). ‘A‘ā lava thus forms leveed channels and increases in viscosity by several orders of magnitude downflow (Moore 1987; Pinkerton and Wilson 1994; Crisp et al. 1994; Baloga et al. 1998).

Pāhoehoe may change to‘a‘ā, but the reverse never occurs in the same material. The transition appears to be controlled by a critical relationship between viscosity and the rate of shear strain (Peterson and Tilling 1980). This relationship is both irreversible and inverse, i.e., lower viscosity lava requires higher rates of strain for the transition to occur. Viscosity is a function of lava composition, temperature, crystallinity, and bubble content. The effect of crystals on rheology is relatively well constrained (at crystal content less than 35–40 vol.%) from both field measurements (Shaw 1969; Pinkerton and Sparks 1978; Pinkerton and Norton 1995) and laboratory experiments on natural samples (Shaw 1969; Ryerson et al. 1988; Spera et al. 1988; Pinkerton and Norton 1995). The effect of bubbles on rheology is much less well constrained, both for natural and experimental studies (see Stein and Spera 1992, and Stone 1994 for reviews). Strain rates are dictated by lava rheology, slope, and eruption rates, and for a given volcano (where erupted lava viscosity is not highly variable) there is an eruption rate above which the flow is ‘a‘ā (Pinkerton and Sparks 1976; Rowland and Walker 1990; Kilburn 1993; Pinkerton and Wilson 1996). Local transitions from pāhoehoe to ‘a‘ā are most commonly the result of local increases in slope (Peterson and Tilling 1980), and they provide the most accessible opportunities to examine the nature of the transition.

Experiments on one-component analog systems (Fink and Griffiths 1990; Griffiths and Fink 1992a, b, 1993; Gregg and Fink 1995) suggest that a simple non-dimensional parameter (ψ) relating time scales of flow advection and flow cooling can be used to predict flow surface morphologies. Advection time (τa), which is defined as the ratio of flow thickness to flow velocity, is the inverse of the vertically averaged shear strain rate through the flow, whereas cooling time (τs) is constant for subaerial lava flows and equivalent to Kilburn’s (1993) chilling time (τch). In theory, the strain rate and viscosity conditions over which the pāhoehoe-‘a‘ā transition occurs can be predicted from observed correlations of lava viscosity and 1/ta, although in practice flow viscosities are, in large part, too poorly constrained to define the conditions of this transition with precision. Thus, the picture that emerges from field observations and experiments is that the transition from a crust-dominated pāhoehoe to a core-dominated ‘a‘ā flow is a complex function of the rheological, thermal properties and fluid dynamics of lava flows. Previous work on the known variation of these properties in lava is summarized herein.

Bubble development and deformation in lava flows

Quantification of bubble populations in lava has been largely limited to studies of easily sampled pāhoehoe flows. Studies of recent pāhoehoe lava from Kīlauea Volcano, Hawai‘i (Walker 1989; Mangan et al. 1993; Wilmoth and Walker 1993; Cashman et al. 1994; Keszthelyi and Denlinger 1996; Cashman and Kauahikaua 1997) have documented the downflow loss of vesicles from active flow surfaces within lava tubes, the pronounced effect of small pressure variations on the bubble population, and the effect of those bubbles on rates of flow cooling. Work on both pāhoehoe and ‘a‘ā from Mount Etna emphasizes the importance of bubble coalescence in generating the final vesicle population (Gaonac’h et al. 1996; Herd and Pinkerton 1997) and introduces the use of bubbles as strain markers in small lava flows (Polacci and Papale 1997).

Studies of the role of bubbles on the rheology of active flows are much more limited. Evidence indicates that bubbles may either increase (Pinkerton et al. 1994; Hon et al. 1994) or decrease (Lipman and Banks 1987) effective flow viscosity. Resolution of these contradictory observations lies in understanding the role of bubble deformation in controlling rheology (e.g., Manga and Stone 1994; Manga et al. 1998). The degree to which bubbles are expected to deform may be expressed as a function of two dimensionless parameters; the capillary number $Ca=(d\gamma/dt)\mu r/\sigma$, where γ is the shear, μ is the melt viscosity, r is the bubble radius, and σ the bubble surface tension (Stein and Spera 1992); and the viscosity ratio λ, which is the ratio between the viscosity of the bubble and that of the melt. Deformation is sub-

stantial in the strong flow regime defined by Ca>0.4. Here bubbles may attain stable shapes and, for high enough shear rates, eventually fragment into numerous daughter bubbles (Bentley and Leal 1986). For Ca<0.4 (weak flow regime, Stein and Spera 1992), bubble deformation is small due to the surface tension forces being greater than viscous forces, and ideally bubbles are deformed into prolate ellipsoids with their long axes oriented 45° to the direction of the flow. The attainment of a stable shape and long axis orientation is a damped oscillation with decay time of approximately $(d\gamma/dt)^{-1}Ca^{3/4}$.

The effect of deformed bubbles on flow rheology depends on the capillary number. For Ca< ~0.5, the effective viscosity of bubbly suspensions is predicted to be a weakly increasing function of vesicularity, and the suspensions show shear thinning behavior (Manga et al. 1998). Experimental results generally support these predictions, with shear-thinning behavior at moderate bubble volume fractions (Stein and Spera 1992), and both increases (Stein and Spera 1992) and decreases (Bagdassarov and Dingwell 1992) in apparent viscosity with small increases in vesicularity (0–25%). Modeling by Manga et al. (in press) suggests that these apparent discrepancies likely reflect both differences in Ca and in durations of transient behavior. Thus, determination of parameters that define Ca (strain rate, melt viscosity, and bubble size) is required for understanding the rheological behavior of bubble-bearing melts.

Application of experimental and theoretical findings on bubble deformation to basaltic lava is limited, and direct investigations of deformed bubbles in lavas and magmas are few. Manga and Stone (1994) explain the alignment of bubbles found in some thick lava flows (i.e., the Cohassett flow of the Grande Ronde basalt, McMillan 1987) as the result of deformation due to hydrodynamic interactions among rising bubbles that lead to horizontal translation that aligns bubbles and enhances coalescence. This mechanism is important in interpreting bubble distributions in lava, where bubble coalescence is common (e.g., Cashman et al. 1994; Gaonac'h et al. 1996; Herd and Pinkerton 1997). A recent investigation of vesicle distributions in lava flows at Mount Etna shows that deformed vesicles provide information on the physical parameters (i.e., strain rates) related to emplacement flow dynamics (Polacci and Papale 1997). The presence of a velocity gradient inside a lava flow induces the deformation of initially spherical bubbles. Bubbles are deformed depending on the flow regime, Ca and viscosity ratio values, and are redistributed according to the local strain rate. Bubble deformations mark changing rheology in lava flows and represent a diagnostic tool for interpreting lava rheology and morphology.

The 1 February 1996 event and the 1868 Mauna Loa eruption

The eruptive event of 1 February 1996 started in the morning with an intense swarm of shallow summit earthquakes, dramatic increase of the summit CO_2/SO_2 gas ratio, and rapid inflation of the summit caldera. Three hours later, a surge of lava reached the active Pu'u 'Ō'ō vent and lava tube system. The tube became overfilled, and dome fountains welled from several skylights along the tube. The largest of these fountains, from the uppermost skylight, was 7.6 m high; it fed a chanellized flow that turned to 'a'ā as it descended through forest on the steep slope of Pūlama Pali. The volume of lava that broke out of the upper skylight on 1 February is estimated to be 4×10^6 m^3 (Thornber et al. 1996), with velocities as high as 18 m/s in the upper third of the flow.

The Mauna Loa activity of 1868 began with a brief summit eruption on 27 March. This was followed by intense seismicity that culminated in a large earthquake on 2 April 1868. The main phase of the eruption started on 7 April and lasted only 4 days. Picritic lava erupted from fissures at elevations of 600–900 m and fed several lava streams, two of which reached the ocean, approximately 18 km from the vent (Lockwood and Lipman 1987). The eruption produced approximately 1.2×10^8 m^3 of lava, for an average mass eruption rate of approximately 300 m^3/s assuming an eruption duration of 4.5 days (Barnard 1990). Flow velocities in the channel were estimated at 5–10 m/s (Barnard 1990), reflecting the high magma supply rates (Rhodes 1995).

Sample description

The samples used in this study were collected at two different locations, one from the Kīlauea flow of 1 February 1996, and the other from the Mauna Loa lava flow of 1868 (Fig. 1). Both flows show a transition from smooth-surfaced pāhoehoe to clinkery 'a'ā across a distance of several tens of meters. The two flows have very different emplacement histories (open channel flow vs temporary storage and effusion from ephemeral vents) and provide the opportunity to study two distinct conditions under which pāhoehoe may change to 'a'ā. As documentation of vesicle deformation was one of the goals of this study, all samples were oriented with respect to the flow direction.

Solidified samples from the 1 February Kīlauea flow (samples KL96/1a, 2, 3 and 4; Table 1) were collected several hundred meters below the Pu'u 'Ō'ō vent, at a point where the channel split into two branches. Here a steepening in the slope caused a transition from pāhoehoe to transitional (poorly developed) 'a'ā. Above the transition point samples have a smooth glassy crust (~0.5 cm thick) with stretched vesicles and lineations in the direction of the flow. At the transition the glassy rind is much thinner (<0.1 cm), and the crust is marked by a rough surface with spines pointing downflow. In addition, a few selected samples of true 'a'ā and pāhoehoe from other locations within the same flow (samples SPT, SKY, 8aL5, 5dL5, 3D1, 4D1) were analyzed for comparison with those samples collected across the transition. Samples from locations closer to the skylight are all pāhoehoe; downflow samples include both pāhoehoe and 'a'ā. All samples analyzed contain between 35 and 74% vesicles, fewer than 2% olivine cystals (long

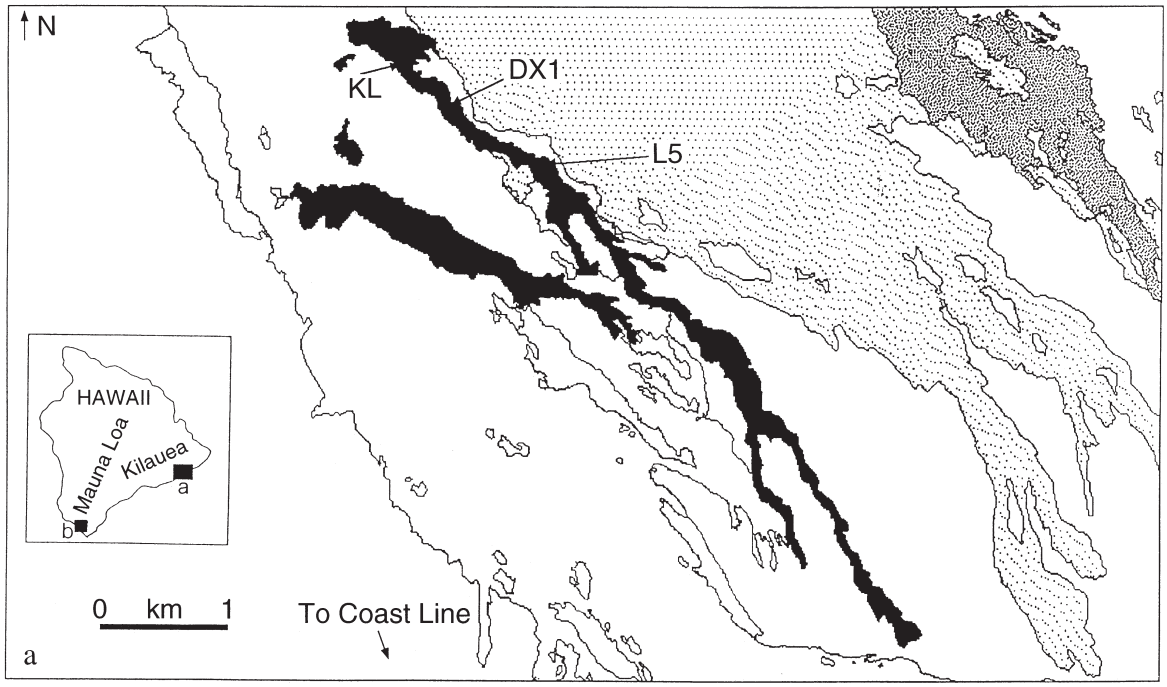

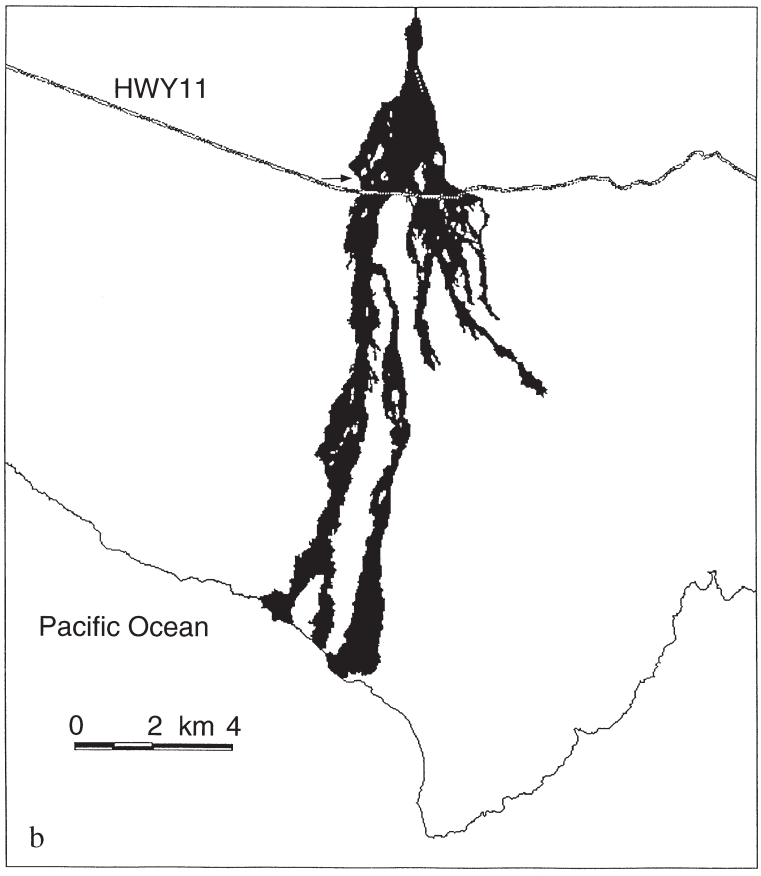

Fig. 1a, b Location maps for **a** the 1 February 1996 event and **b** 1868 Mauna Loa eruption. In **a** the 1 February event is in *black* and *KL*, *DX1*, and *L5* are locations of, respectively, samples KL1/KL2/KL3/KL4, 3D1/4D1, 5dL5/8aL5. *Dotted areas* represent lava fields from Kilauea's ongoing eruption. General Big Island map is also inserted. In **b** *arrow* shows the location of samples studied for the 1868 Mauna Loa eruption. Highway 11 is also indicated

axis generally <0.1 cm), and abundant microlites and microphenocrysts in the groundmass.

Samples from the 1868 Mauna Loa eruption (samples ML68/4, 5, 6a, 6b, 7, 8, 9a, 10a, C1, C2; Table 1) belong to an ephemeral vent located at the center of one of the main channels near the point where the flow crosses Highway 11 on the south coast of Hawai'i. The ephemeral vent is subdivided into zones with different surface morphologies, as de-

Table 1 Sample description

Kīlauea 1 February 1996 flow

Sample no.	Distance from the pāhoehoe/ʻaʻā transition	Description
KL96/1a	60.0 m before the transition	Shelly pāhoehoe
KL96/1b	60.0 m before the transition	Second layer/shelly pāhoehoe
KL96/2	Transition sample	Pasty pāhoehoe
KL96/3	15.0 m below the transition	Transitional slab pāhoehoe
KL96/4	40.0 m below the transition	Transitional slab pāhoehoe

Kīlauea 1 February 1996 flow

Sample no.	Distance from 2450 skylight	Description
KL96/SPT	0	Spatter vent sample
KL96/SKY	200.0	Shelly fountain-fed pāhoehoe
KL96/3D1	1000.0	Transitional slab pāhoehoe
KL96/4D1	1000.0	Clinkery ʻaʻā
KL96/5dL5	2000.0	Shelly pāhoehoe from eastern levee of channel
KL96/8aL5	2000.0	Dense slab of rough pāhoehoe

Mauna Loa 1868 eruption

Sample no.	Distance from the ephemeral vent (m)	Description
ML68/4	15.0 before the vent	Smooth pāhoehoe
ML68/C	0	Smooth pāhoehoe
ML68/5	3.8	Rough pāhoehoe
ML68/6a	10.2	Rough pāhoehoe
ML68/6b	10.2	Smooth pāhoehoe
ML68/9a	18.4	Smooth pāhoehoe
ML68/10a	18.4	Rough pāhoehoe
ML68/7	45.7	Clinkery ʻaʻā
ML68/8	49.4	Clinkery ʻaʻā

scribed by Polacci and Papale (1997) for the ephemeral vents at Mount Etna. A complete transition from pāhoehoe to ʻaʻā morphology may be followed for at least 50 m from the emission point. In the transition, lava with an initially smooth pāhoehoe crust becomes rougher as the flow turns progressively to ʻaʻā. Locally the transitional portion of the flow has smooth and rough pāhoehoe slabs coexisting at the same location (samples 6a and 6b, 9a, and 10a). All samples show the same range of microlite and microphenocryst numbers and total crystallinities in the groundmass as do the Kīlauea samples, slightly lower (27–67%) vesicle contents, and up to 25% olivine phenocrysts (long axis ≤ 0.7 cm).

Methods

To determine the three-dimensional morphology of vesicles, samples were cut along three mutually perpendicular planes oriented (a) along the flow direction, (b) across the flow direction, and (c) parallel to the flow surface. At least one oriented thin section was made from each of these sections for each sample. Images of samples were obtained directly from thin sections by capturing a full section image with a video camera. Vesicularities (area fraction of vesicles), vesicle number densities (the number of vesicles per unit area), individual vesicle areas, and phenocryst contents were measured from binary images created from the scanned sections (Russ 1986) using NIH Image and Dapple sofware. Direct measurements of vesicle areas and shapes were converted to equivalent diameter (the diameter of a circle the area of which is equivalent to the area of the vesicle), deformation parameter D=(l-b)/(l+b), where l and b are major and minor axes of vesicles (Taylor 1934), and orientation angle.

Thin sections preserving glass from flow crusts were later polished for backscattered electron (BSE) imaging. The absence of preserved glass in the ʻaʻā limited textural analysis of glassy areas to pāhoehoe and transitional morphologies. The BSE images were collected from polished thin sections on a JEOL JSM-6300 V SEM, at an accelerating voltage of 10 kV, a working distance of 15 mm, and 500 magnification. Microlite (<30 μm) and microphenocryst (between 30 and 100 μm) number densities (number of crystals per unit area) were measured on the digital images. Microlite and microphenocryst crystallinities (area fraction of crystals) were obtained from the same images by automated analysis (where grayscale contrasts permitted) or by manually point-counting the BSE images. All groundmass textural parameters were calculated free of vesicles and phenocrysts by eliminating the area fraction of the image occupied by these phases. This allowed us to consider the melt fraction available at the time of microlite and microphenocryst growth. Samples with higher microlite and microphenocryst crystallinities (>30% crystals) required images at both 500 and 250 magnification to cover a representative area and to ensure identification of the features of interest. Very small pyroxene crystals (<1 μm) were difficult to identify unambiguously; thus, number density measurements of very small pyroxene microlites are considered minimum values. Number densities and abundance of both crystals and vesicles are reported for each oriented thin section as actual two-dimensional data. We chose to do this as we believe it provides a reasonable way to compare textural characteristics between samples. Average vesicle diameter d can be calculated from measured areal number density (Na) and area fraction (Ø) as $d = S\sqrt{Ø / Na}$, where S is a shape factor. The volumetric number density (Nv) can then be estimated as Nv=Na/d.

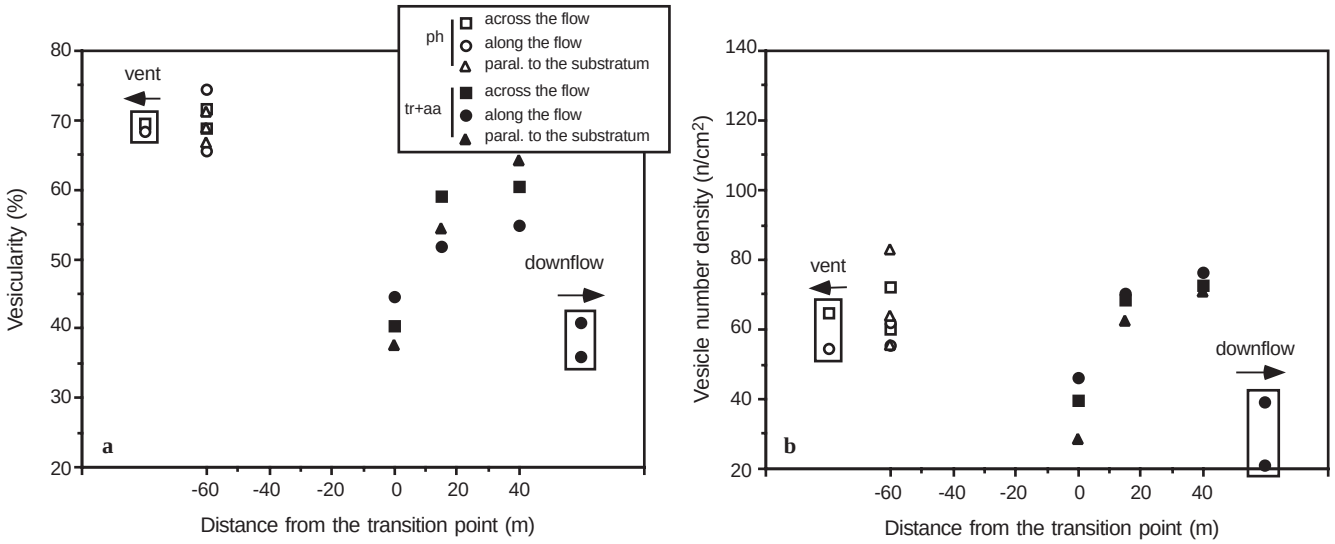

Fig. 2 **a** Vesicularity and **b** vesicle number density for Kilauea samples. Points at the same distance from the transition come from the same sample and refer to different sample orientations: *squares* across-flow direction; *circles* along-flow direction; *triangles* direction parallel to the flow surface. *Open symbols* refer to pāhoehoe samples, *filled symbols* to transitional and ‘a‘ā samples. See text for further explanation

Results

Textural characteristics

Vesicles

Figure 2 shows vesicularity and vesicle number density patterns across the Pāhoehoe-‘a‘ā transition for the Kīlauea samples examined. Vesicularity and vesicle number density are highest before the transition, at 65–74% and 55–83 cm^{-2}, respectively. Both measurements show a net decrease at the transition point (to 37–44% and 28–46 cm^{-2}) but increase again to 51–64% and 62–76 cm^{-2} over the next 30 m. Bracketing textural measurements from near-vent and distal samples are shown in rectangular boxes . Near-vent shelly pāhoehoe (sample SKY), with measured vesicularities of 69% and number densities of 60 cm^{-2}, most closely resembles the pre-transition Pāhoehoe, but the distal clinkery ‘a‘ā (4D1, 8aL5) samples show diminished vesicularities (38%) and vesicle number densities (30 cm^{-2}) similar to those of the transition sample. Spatter vent sample (SPT) is heterogeneous in vesicularity and is characterized by very round vesicles.

Samples from Mauna Loa show a similar range in vesicularities (27–68%) and similar to slightly higher vesicle number densities (20–124 cm^{-2}) as are in the Kīlauea samples. Again, overall sample vesicularity decreases substantially across the transition (Fig. 3a). However smooth pāhoehoe samples at 10.2 m (6b) and 18.4 m (9a) from the ephemeral vent provide exceptions to this generalization. The vesicularity of these samples ranges between 61 and 68% and is higher than that of transitional lava sampled at

Fig. 3 **a** Vesicularity and **b** vesicle number density for Mauna Loa samples. Symbols as in Fig. 2. See text for further explanation

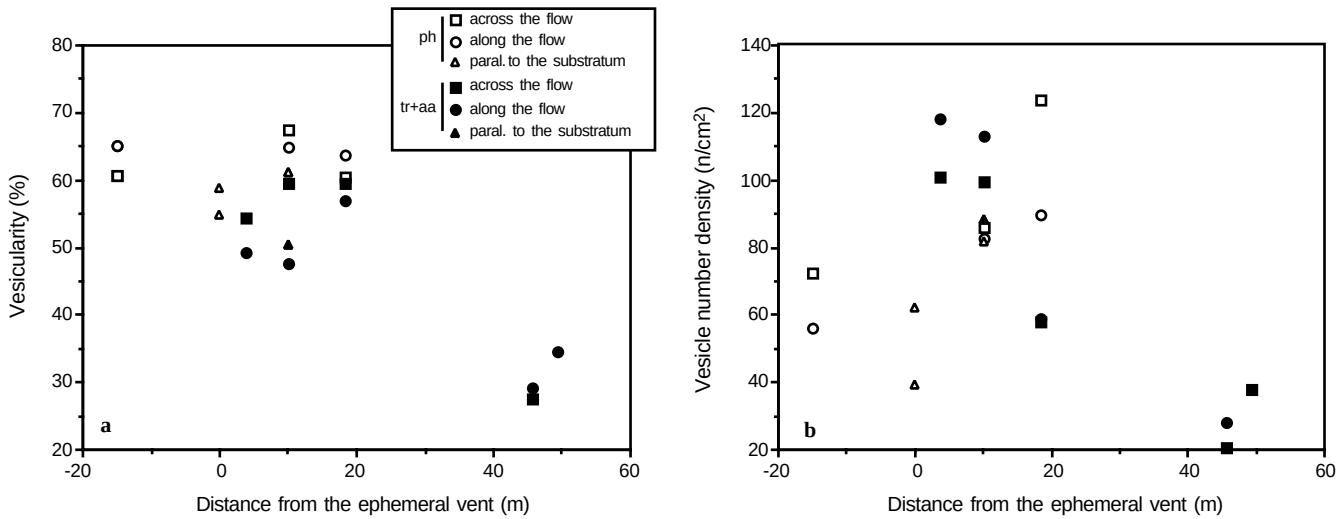

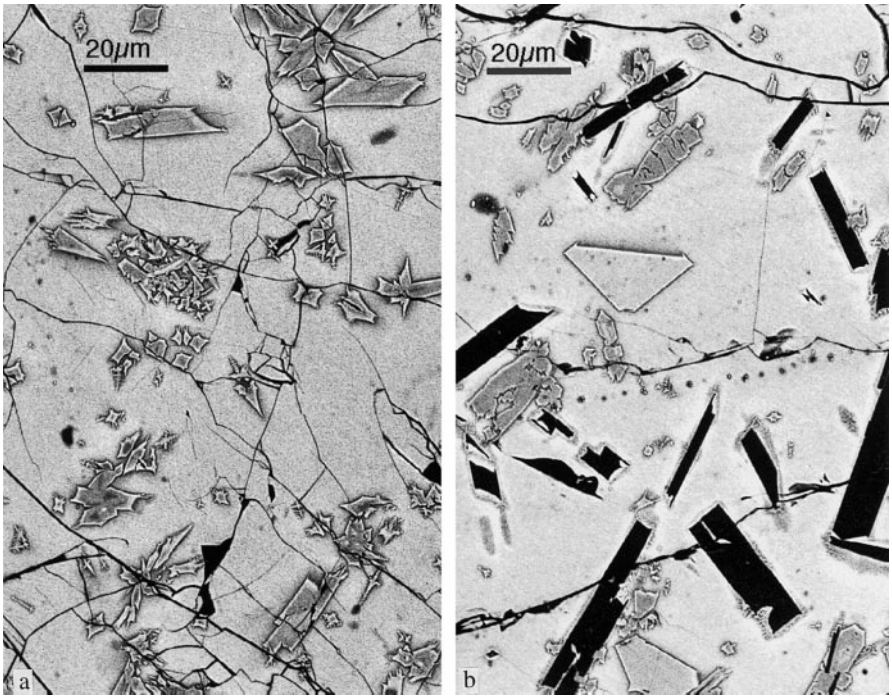

Fig. 4a, b Backscattered electron (BSE) images of samples KL96/1a, 2. **a** *Dark-gray crystals* are pyroxene microlites and *black features* are fractures. **b** *Dark-gray crystals* are pyroxene microlites, *light-gray crystals* are olivine, and *black crystals* are plagioclase microlites and microphenocrysts

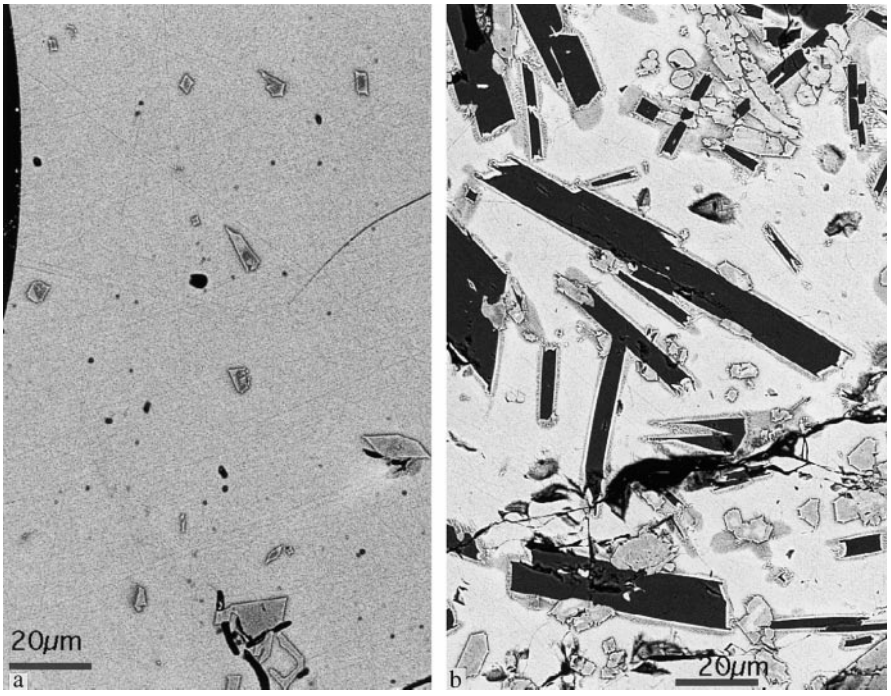

Fig. 5a, b The BSE images of samples ML68/6b, 6a. **a** *Dark-gray* features are pyroxene microlites, *black features* are vesicles. **b** *Dark-gray features* are pyroxene microlites, *black crystals* are plagioclase

the same location. The spherical shape and overall size distribution of the vesicles in these smooth pāhoehoe samples are similar to those described from small breakouts from advancing pāhoehoe flows (e.g., Cashman et al. 1994) and suggest that these samples had a similar origin. Vesicle number densities are generally high (~110 cm^{-2}) in the transition samples, increasing from pre-transition values (~60 cm^{-2}) and decreasing again by 45 m downflow (to ~20 cm^{-2}) as a complete morphological transition to clinkery ‘a‘ā is achieved (Fig. 3b).

Groundmass crystals

Groundmass crystallinity increases dramatically as flow surfaces change from smooth to torn crust (Figs. 4, 5). In general, Kīlauea spatter vent samples are microlite free, smooth pāhoehoe samples have low to moderate crystallinities (0–14%), and distal transitional samples have high (27–30%) groundmass crystallinities (Fig. 6a). Trends in crystal number density generally mirror those of crystallinity, with pyroxene microlites more numerous than pla-

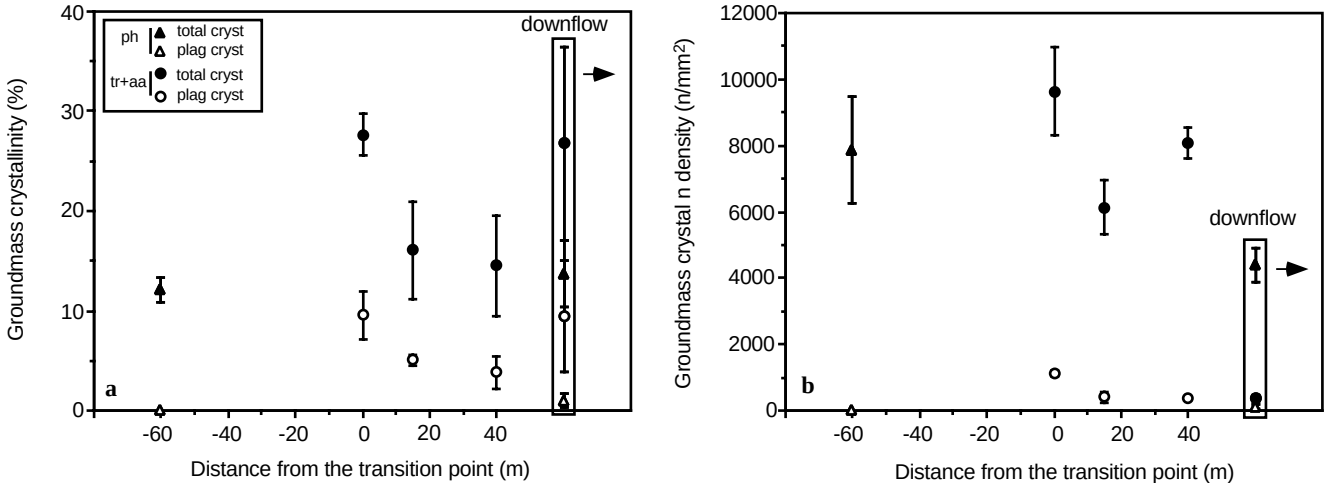

Fig. 6 **a** Groundmass crystallinity and **b** crystal number density for Kilauea samples. *Triangles* represent pāhoehoe morphology, circles ʻaʻā or transitional morphology. *Closed symbols* refer to total values, *open symbols* to plagioclase values. Standard deviation *error bars* are shown. See text for further explanation

gioclase (Fig. 6b), although crystal number density measurements were complicated by abundant quenched pyroxene microlites (<1 μm long; see Methods). However, in detail, samples immediately upflow and downflow from the transition have similar groundmass crystallinities (12–16%, distinct from the 28% groundmass crystallinity at the transition) and crystal number densities (7861–6136 mm^{-2}), except that plagioclase (5% and 400 mm^{-2}) is present only in downflow samples.

Measured variations in crystallinity in Mauna Loa samples are comparable to those of the Kīlauea flow (Fig. 7a), although crystal number densities (Fig. 7b) are approximately half those of Kīlauea samples. As crystal number density and crystal volume fraction are related through average crystal size, this observation indicates that the Mauna Loa microlites are, on average, larger than those of Kīlauea. Again, both crystallinity and crystal number density are consistently higher for the transitional samples than for the smooth pāhoehoe. As seen in the Kīlauea samples, pyroxene nucleation clearly precedes that of plagioclase (Figs. 4–7; see Table 3), and plagioclase crystallinity and microlite number density are always less than those of pyroxene.

Vesicle deformation measurements

The vesicle deformation parameter D may be directly correlated with capillary number Ca when Ca (and D) <0.4, and thus for small strains (low D) measurements of D can theoretically provide estimates of strain rates accompanying lava emplacement (Stein and Spera 1992). Vesicle deformation parameters D were calculated for each of the samples from measured values of vesicle length and width. D ranges from 0 (spherical) to 0.7 (ellipsoidal), but most of the measured D values are below 0.4. A mean value of D was then calculated for each thin section (Table 2); values range from 0.166 to 0.266 for the Kīlauea flow and from 0.193 to 0.294 for the Mauna Loa flow. D is consistently

Fig. 7 **a** Groundmass crystallinity and **b** crystal number density for Mauna Loa samples. Symbols as in Fig. 6. Standard deviation *error bars* are shown. See text for further explanation

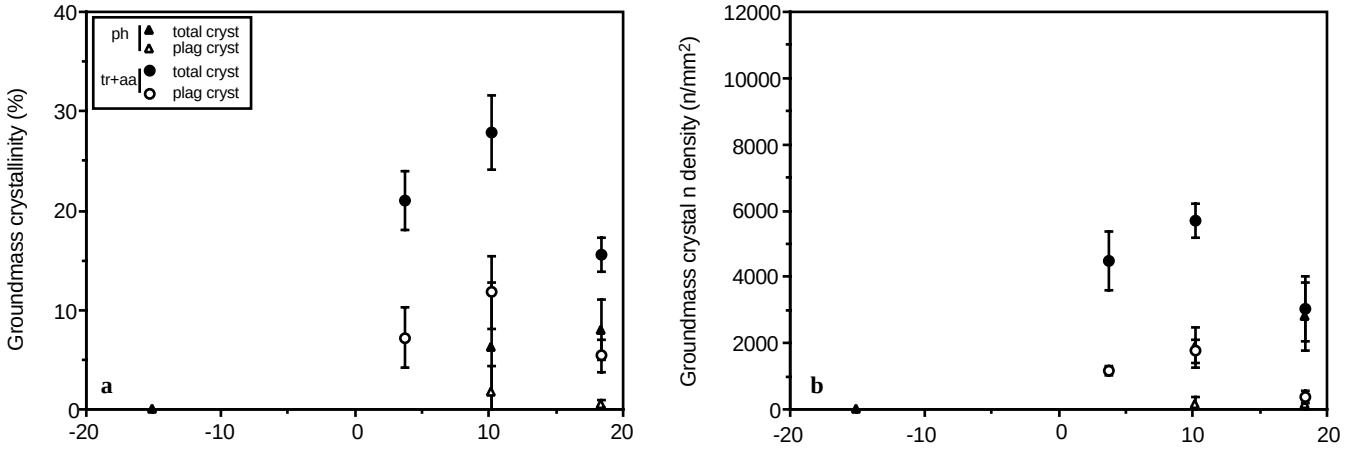

Table 2 Vesiculation measurements. *nF* perpendicular to flow direction; *pF* parallel to flow direction; *h* parallel to flow surface

Sample no.	Number measured	Vesicularity (%)	Vesicle number density (cm^{-2})	Vesicle deformation parameter[a]
Kīlauea samples				
KL96/1anF	518 (310)[b]	71.5 (68.8)[b]	60.2 (72)[b]	0.203
KL96/1apF	301 (440)[b]	74.5 (65.4)[b]	55.2 (61.7)[b]	0.203
KL96/1ah1	175	71.1	63.8	0.166
KL96/1ah2	328	66.6	82.6	0.174
KL96/1ah3	231	68.7	55.4	0.194
KL96/2nF	231	40.4	39.4	0.243
KL96/2pF	423	44.4	46.1	0.224
KL96/2 h	166	37.5	28.4	0.203
KL96/3nF	365	58.9	68.2	0.215
KL96/3pF	540	51.7	70.1	0.232
KL96/3 h	275	54.3	62.2	0.203
KL96/4nF	567	60.4	72.4	0.210
KL96/4pF	421	54.8	76.2	0.217
KL96/4 h	174	64.0	70.9	0.211
KL96/SKYnF	397	69.4	64.7	0.224
KL96/SKYpF	333	68.5	54.4	0.231
KL96/4D1pF	276	40.7	39.3	0.255
KL96/8a5L5	177	35.8	20.8	0.266
Mauna Loa samples				
ML68/C1	200	58.6	62.1	0.234
ML68/C2	118	54.7	39.3	0.214
ML68/4nF	387	60.7	72.5	0.230
ML68/4pF	263	65.0	56.0	0.240
ML68/5nF	571	54.3	118.0	0.271
ML68/5pF	720	49.2	100.7	0.294
ML68/6anF	846	59.4	112.8	0.277
ML68/6apF	417	47.5	99.5	0.265
ML68/6ah	289	50.4	88.3	0.244
ML68/6bnF	402	67.5	85.7	0.221
ML68/6bpF	619	64.8	82.4	0.221
ML68/6bh	163	61.2	81.5	0.196
ML68/7nF	196	27.3	28.1	0.193
ML68/7pF	117	29.2	20.2	0.208
Ml68/8pF	210	34.5	37.7	0.221
ML68/9anF	301	61.2	123.6	0.250
ML68/9apF	679	63.6	89.5	0.243
ML68/10nF	380	59.5	58.6	0.258
ML68/10pF	368	57.0	57.8	0.263

[a]Average value of D for each series (see text for further explanation)
[b]Values in parentheses refer to another slice from the same sample

smaller for measurements made on the plane parallel to the flow surface (Table 2, samples KL96/1a, 2, 3, 4, and ML68/6a, 6b). The highest deformation values can be found either parallel or perpendicular to the flow direction, with a slight predominance of the parallel (samples KL96/3,4,SKY and ML68/4,5,7,10).

Transitional and clinkery ʻaʻā samples are characterized by higher mean D values than are smooth pāhoehoe samples (Table 2). This is illustrated in binary images of vesicles (Figs. 8, 9), in which samples with pāhoehoe morphologies (Figs. 8a, 9a) have more spherical (less deformed) vesicles than samples with transitional morphologies (Figs. 8b, 9b). This observation is also supported by data presented in Fig. 10, where mean D values are compared with sample vesicularity. For both the Kīlauea and Mauna Loa flows, there is a general trend of increasing vesicle deformation with decreasing vesicularity, and samples showing transitional and clinkery ʻaʻā morphologies have more deformed vesicles than do Pāhoehoe samples. Exceptions (framed in their corresponding figures) are a highly vesicular vent sample (KL96/SKY) showing moderate vesicle deformation and clinkery ʻaʻā samples (ML68/7 and 8). The pāhoehoe vent sample is characterized by deformed and elongated vesicles (average D=0.227), which may reflect high strain rates occurring at the vent region at the time of effusion. The clinkery ʻaʻā samples show an overall decrease in D value with decreasing vesicularity. Careful observations of thin sections of these samples show that the vesicles have adopted convoluted shapes in response to the lack of space created by the high olivine phenocryst crystallinity (Fig. 11). These irregular shapes are not adequately represented by a simple calculation of D. Mean D values also show an overall increase with increasing bulk crystallinity (Fig. 12). Kīlauea samples have lower D values than do Mauna Loa samples with similar groundmass crystallinities, perhaps a consequence of the higher total crystallinities in the Mauna Loa samples. However, although measured variations in D could reflect true varia-

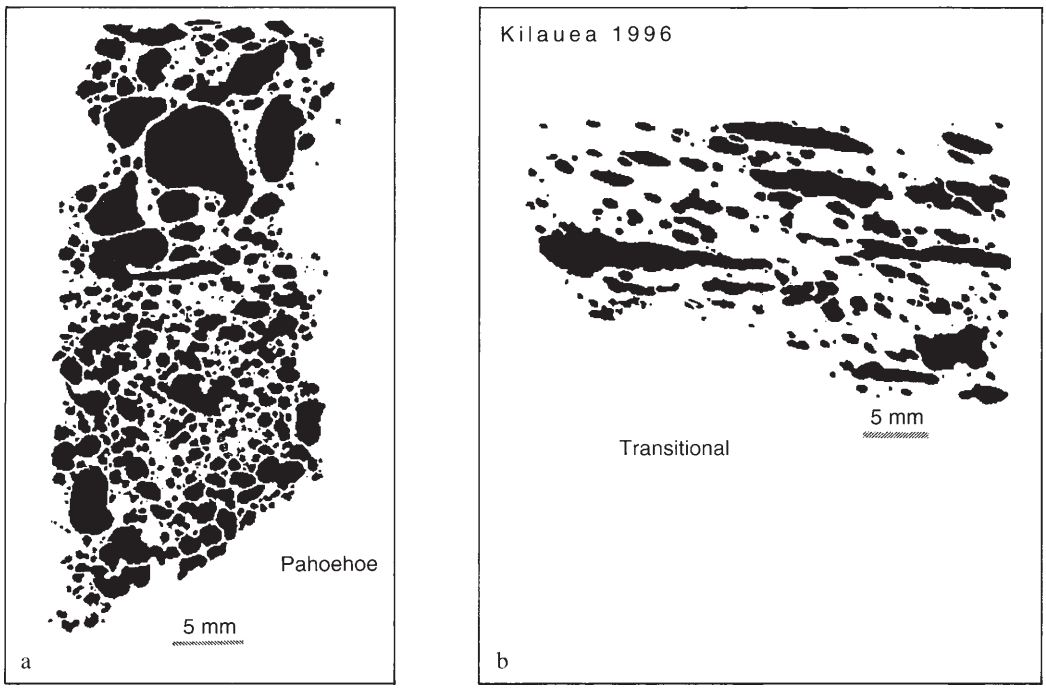

Fig. 8a, b Binary images of samples **a** KL96/1a and **b** KL96/2. Vesicles are *black features*, glass plus microlites are *white*. Phenocrysts are not shown. **a** Vesicles tend to be relatively undeformed in the Pāhoehoe sample (KL96/1a); **b** vesicles assume elongated and more deformed shapes (slightly ellipsoidal) in the transitional sample (KL96/2)

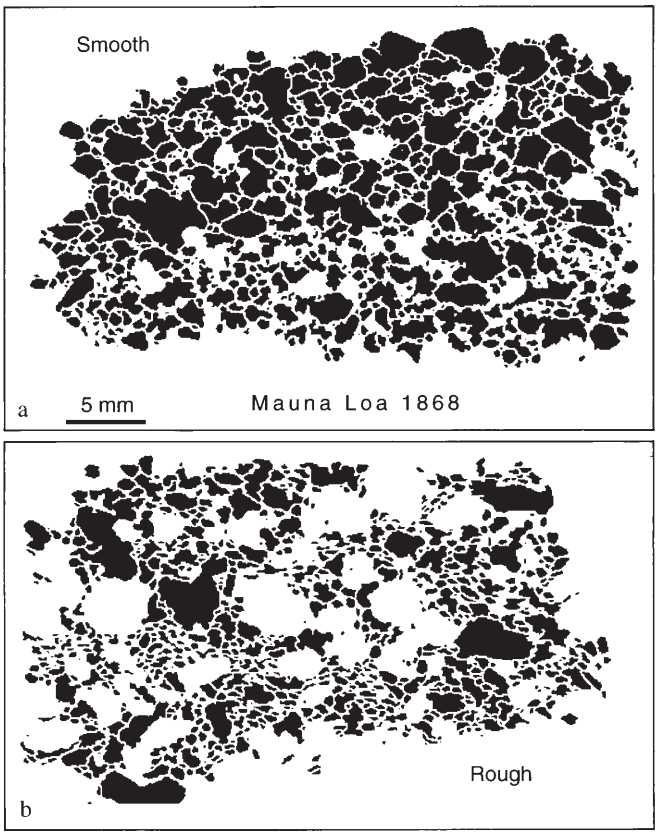

Fig. 9a, b Binary images of samples **a** ML68/6b and **b** ML68/6a. Vesicles are more deformed in the rough sample morphology than in the smooth sample morphology. Scale bar is the same for both images

tions in Ca, we note that none of the vesicles preserved in our samples has a pointed tip, indicating that partial relaxation of bubble shape occurred in all samples. Moreover, as relaxation time is partly a function of melt viscosity, relaxation of bubble shapes might have occurred more quickly in the less viscous (less crystalline) lavas.

Discussion

In both flows, the transition in flow surface morphology from pāhoehoe to transitional ʻaʻā is generally accompanied by: (a) a decrease in total vesicularity and vesicle number density; (b) an increase in microlite crystallinity and crystal number density; and (c) an increase in the amount of vesicle deformation. However, in detail, patterns of both vesicularity and crystallinity are complex, with local variations likely a function of exactly how the transition was preserved as flow ceased. These results are similar to measurements made by Lipman and Banks (1987), Crisp et al. (1994), and Cashman et al. (1997) on samples collected from recently active ʻaʻā flows. They demonstrate that both increasing crystallinity and decreasing vesicularity are expected consequences of lava flow under conditions responsible for generation of transitional to ʻaʻā surface morphologies. These data are preliminary, but none the less the measurements presented previously can be extended to provide quantitative constraints on conditions accompanying the pāhoehoe-ʻaʻā transition. Below we examine the implications of the textural results for quantification of rheologic changes to lava during flow emplacement.

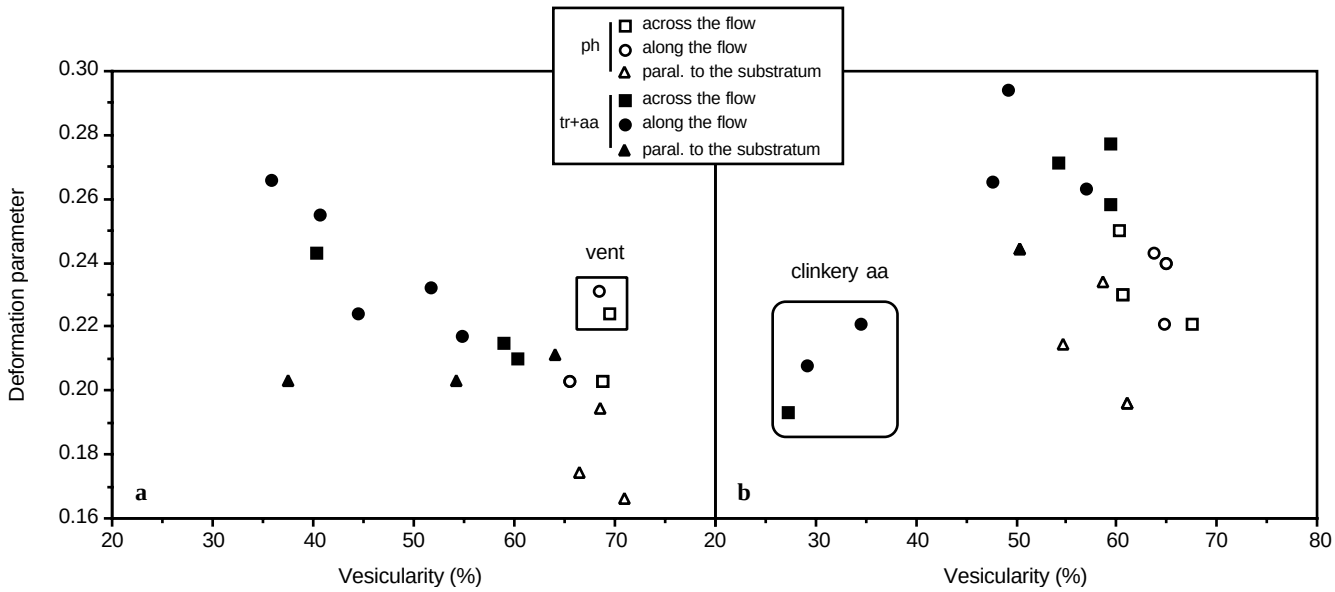

Fig. 10a, b Deformation parameter vs vesicularity for **a** all Kilauea and **b** all Mauna Loa samples. Standard deviation *error bars* are shown. Symbols as in Fig. 2

Fig. 11 Modified binary image of sample ML68/7. Vesicles are *white features*, glass plus microlites are *black*, and olivine phenocrysts are *dark gray*. Note how vesicles assume convoluted shapes as they tend to adjust among olivine crystals

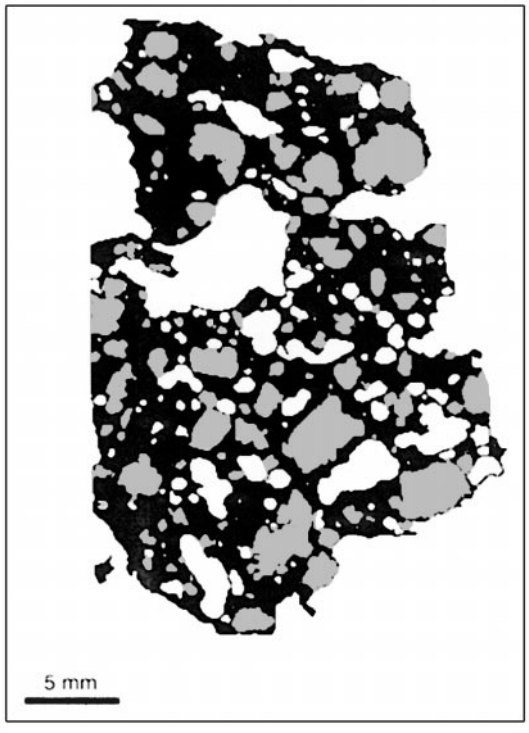

Textural changes with flow

Bubble loss during flow has been documented both in active Hawaiian pāhoehoe (Cashman et al. 1994; Hon et al. 1994) and ʻaʻā (Lipman and Banks 1987) flows and has also been inferred from vesicularity observations on solidifed samples of flows of both types (e.g., Macdonald 1953; Wilmoth and Walker 1993). Vesicularity decrease in pāhoehoe flows has been attributed primarily to bubble loss at flow surfaces, although resorption resulting from pressure increases at flow bases has been suggested for unusually fluid flows emerging from temporary storage in inflat-

Fig. 12 Average value of D vs bulk crystallinity for the Kilauea (*squares*) and Mauna Loa (*circles*) flows. Standard deviation *error bars* are shown

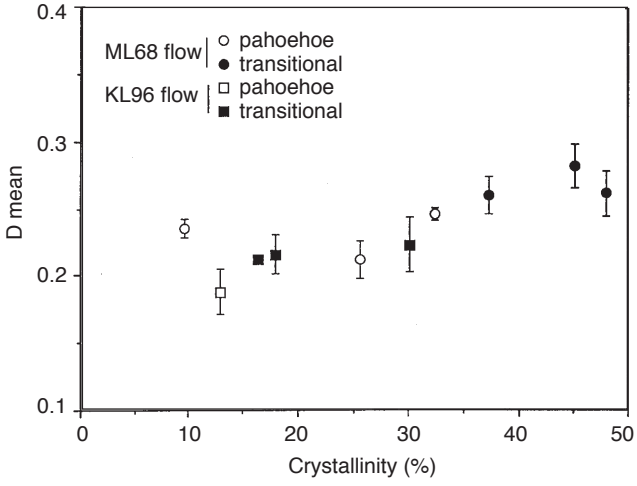

Table 3 Crystal measurements

Sample no.	Number measured[a]	Crystallinity (%)[b]	Plagioclase crystallinity (%)[b]	Crystal number density (mm^{-2})	Plagioclase number density (mm^{-2})	Phenocryst crystallinity (%)
Kīlauea samples						
KL96/1a	727	12.0	0	7860.6	0	0.3
KL96/2	2057	27.6	9.5	9626.8	1131.1	2.1
KL96/3	1653	16.0	5.0	6136.3	399.0	1.1
KL96/4	1273	14.5	3.7	8077.9	373.3	1.1
KL96/SKY						0
KL96/4D1						1.3
KL96/8aL5						2.0
KL96/3D1	201 (only plagioclase)	26.7	9.4	366.0		
KL96/5dL5	1093	13.7	0.9	4376.0	108.0	
Mauna Loa samples						
ML68/4	0	0	0	0	0	9.6
ML68/5	635	21.0	7.2	4480.6	1174.4	14.7
ML68/6a	712	27.8	11.7	5697.3	1760.4	13.3
ML68/6b	386	6.2	1.6	1871.2	144.2	7.4
ML68/7						22.9
ML68/8						23.6
ML68/9a	337	8.0	0.5	2810.4	141.3	10.0
ML68/10a	613	15.5	5.3	3035.1	369.1	10.8

[a]Sum of all microlites measured in each sample
[b]Microlite crystallinity calculated as the ratio between the area percentage of microlites and the area percentage occupied by microlites plus glass. All values have been measured as average values for each sample

ing flows (Hon et al. 1994). In contrast, the near absence of vesicles characteristic of distal ʻaʻā is more commonly attributed to shearing and bubble collapse aided by the greater flow thicknesses and higher viscosities typical of ʻaʻā (Lipman and Banks 1987). Data presented here are consistent with the latter interpretation. In both flows vesicularity decreases from ~65–70% to <30% over distances as short as 50 m. Accompanying decreases in vesicle number density could result from a number of different processes, but the relatively high values of the vesicle deformation parameter in transitional samples suggest gas loss through a permeable network and subsequent bubble collapse to be the most likely explanation, with bubble deformation increasing permeability and aiding gas escape (e.g., Saar and Manga 1999). Vesicle deformation is always smaller on the plane parallel to the flow surface. Alignments of vesicles along a preferential orientation suggest a simple stress tensor acting on the flow, as coalescence would hinder a preferred direction of vesicles.

The correlation of groundmass crystallinity with surface morphology is more dramatic than simple correlations with distance from vent. Samples from the ephemeral vent within the channel of the Mauna Loa 1868 flow are particularly striking in this regard (Fig. 7; Table 3). Here lava effusion following temporary storage within the channel produced flow lobes with both smooth and rough (transitional) pāhoehoe surfaces to distances <20 m from the vent, with total transition to ʻaʻā achieved at a distance less than <50 m from the ephemeral vent. Samples from smooth pāhoehoe surfaces have less than ~10% total microlite crystallinity and <2% microlitic plagioclase (<150 mm^{-2}), whereas those with rough pāhoehoe surfaces have >15% microlite crystallinity and >5% plagioclase microlites (>350 mm^{-2}). The smooth pāhoehoe samples also have <10% olivine phenocrysts, whereas the rough pāhoehoe have >10% olivine phenocrysts. The difference in phenocryst content of the surface crust likely reflects differences in olivine settling rates resulting from flow viscosity changes with increasing groundmass crystallinity (e.g., Rowland and Walker 1987), but the correlation of microlite content with degree of surface roughness suggests that these two features may be related. Comparison with the Kīlauea samples (Fig. 6; Table 3) suggests that plagioclase microlites, more than total bulk or microlite crystallinity, may lead to transitional flow surface textures (see also Kilburn 1990). Samples with <1% plagioclase microlites have smooth textures despite 12–14% pyroxene microlites, whereas those with >4% plagioclase have pasty or transitional surface textures; plagioclase number densities are similar in both types to those of the Mauna Loa samples. Thus, we tentatively conclude that the abundance of platy plagioclase microlites may play a critical role in determining flow surface textures under conditions where crustal rupture is sufficient to expose the surface lava to high stresses (Cashman et al. 1997).

Crystallization kinetics

Microlite textures preserved in quenched (glassy) flow surfaces also provide insight into the kinetics of post-eruption crystallization. Two interesting points emerge from contrasting the very high velocity emplacement of the 1996 Kīlauea flow with the (presumably) lower flow velocities of the late-stage Mauna Loa flow from an ephemeral vent. Firstly, both sample sets show evidence for a slight to substantial delay in the nucleation of plagioclase relative to pyroxene. This delay is particularly apparent in the pre-transition Kīlauea sample, which has a very high amount of pyroxene, all of which grew during transport through the open channel (based on the absence of microlites in vent samples KL96/SKY, KL96/SPT), and only a trace amount of plagioclase. A measure of this delay is provided by pyroxene/plagioclase volumetric abundance ratios, which range from 16 to 4 in all smooth Pāhoehoe samples, whereas those of transitional samples are ~3. Delay of plagioclase nucleation is well know from experimental studies on lunar basalt (Walker et al. 1978) but is less pronounced in terrestrial basaltic systems, except under conditions of very high cooling rates (~100°C/h; Lesher et al., in press) or for a difference of a few tens of degrees in the initial-melting temperature of lava near the liquidus temperature (Sato 1995).

A second point of interest is the extraordinarily high microlite number densities observed in the 1996 Kīlauea samples (Table 3). Crystal number densities increase with increasing rates of supersaturation, and, when calibrated, can be used to estimate rates of cooling in basaltic systems (Cashman 1993). The extent to which nucleation is aided by high strain rates (Kouchi et al. 1986) has never been fully quantified. Measured values in excess of 8000 mm^{-2} are high relative to published crystal number density measurements for the ʻaʻā flow produced by Mauna Loa in 1984 (Crisp et al. 1994) and to those of a small channel-fed ʻaʻā flow from Kīlauea sampled in May 1997 (Cashman et al. 1997). The extremely high pyroxene nucleation rates implied by these data, together with the dramatic delay in plagioclase nucleation, are most easily attributed to very high rates of initial cooling produced by high rates of crustal disruption and stirring within the rapidly flowing channel lava (as for the 1 February 1996 flow). Both plagioclase and pyroxene number densities in the Mauna Loa 1868 samples more closely resemble those of the above referenced studies and appear to reflect more typical rates of cooling (10–50°C/h; Cashman et al. 1997) and crystallization (~30 vol.%/h) in near-vent portions of open channel flows.

Vesicles as recorders of strain rate

Vesicles in pāhoehoe tend to be spherical, whereas those in ʻaʻā are commonly highly deformed (Macdonald 1953; Polacci and Papale 1997). Moderate bubble deformations (D<0.4) reflect moderate Ca numbers, and under these conditions we have pointed out that D can be directly equated with Ca. This raises the possibility of using measured vesicle shapes, together with vesicle size and estimates of flow viscosity, to determine strain rates. Firstly, however, questions of preservation must be addressed.

When bubbles deform, they have pointed tips (Stein and Spera 1992). Bubbles relax by re-rounding, which first affects the tips with their very high radii of curvature. True pointed tips are rare to nonexistent in deformed vesicles preserved in basalt, suggesting that all have undergone some degree of re-rounding and relaxation. Thus, strain rates estimated from measured bubble deformations are minimum values. Time scales of re-rounding (τ) can be estimated from bubble radius (r) and melt surface tension and viscosity, $\tau = r\mu/s$. Calculated re-rounding times are <1 s for small (1 mm) bubbles and low (100 Pa s) melt viscosities. However, increasing crystallinity in a flow results in increasing bulk viscosity (Gay et al. 1969; Shaw 1969; Pinkerton and Stevenson 1992; Pinkerton and Norton 1995), which for crystallization of <30% will likely be more important than the effects of changing temperature and composition of the liquid (Crisp et al. 1994; Montierth et al. 1995). Simple application of the modified Einstein-Roscoe equation (Marsh 1981; Pinkerton and Stevenson 1992) suggests that viscosity increases up to five times as the result of increasing crystallinity alone. This will serve to increase time scales required for bubble relaxation and suggests that, in part, the more highly deformed vesicles preserved in transitional to ʻaʻā flow morphologies may reflect the higher flow crystallinities (and thus viscosities) of ʻaʻā rather than particularly high strain rates.

Given the limitations imposed by the relaxation times calculated herein, measured vesicle deformations can still be used to place constraints on strain rates in lava flows. Minimum strain rates estimated from vesicle deformations are between 1 and 0.1/s. These strain rates are reasonable, although they are somewhat lower than maximum estimates of ~5–10/s derived from velocity and depth measurements (Fink and Griffiths 1990) on active flows (Lipman and Banks 1987). Thus, vesicle deformation measurements, when coupled with characterization of the matrix viscosity, can be used to obtain reasonable minimum estimates of strain rate.

Conclusion

As noted by Macdonald (1953) and Peterson and Tilling (1980), the transition of lava surface morphologies from pāhoehoe to ʻaʻā can occur under a variety of physical conditions. Two of these (open channel flow and remobilization of material from ephemeral vents) have been studied herein. In both cases the transition to ʻaʻā involves (a) an increase in microlite crystallinity and number density of the groundmass, (b) a decrease in vesicularity and vesicle number density, and (c) an increase in the vesicle deformation parameter D. All of these textural changes can be quantified and interpreted in the context of the dynamics of flow emplacement. Changes in microlite crystallinity provide a measure of the extent to which cooling has occurred in the flow, whereas crystal number densities

(and, in a general sense, the degree to which plagioclase nucleation is delayed) can be used to estimate the rates at which that cooling occurred. Increasing groundmass crystallinities will, in turn, increase lava viscosity and change the response of the flow surface to deformation. Increasing crystallinities will also affect the overall rheologic behavior of the flow and provide a link between small-scale textural features and macroscopic changes of lava morphology, such as the larger-scale autobrecciation characteristic of the pāhoehoe–ʻaʻā transition. Flow surface morphologies are not as sensitive to the olivine phenocryst content, an observation that led Peterson and Tilling (1980) to the conclusion that flow morphology was not directly related to crystallinity.

Changes in vesicularity and vesicle size and shape can be used to estimate rates of gas loss and/or resorption within the flow, and they may ultimately contribute information on the development of permeability within ʻaʻā flows. Preserved vesicle deformations provide minimum estimates of flow strain rates for conditions of low capillary number (Ca), in addition to recording distributions of strain across flow lobes (Polacci and Papale 1997). Thus, the transition of lava from pāhoehoe to ʻaʻā surface morphologies and emplacement styles involves numerous textural and rheologic changes within the melt, all of which provide some record of the active process.

Acknowledgements This work was supported by a grant from the University of Pisa to M.P., and by NSF grant EAR9508144 to K.V.C. We thank the Hawaiian Volcano Observatory (particularly F. Trusdell) for assistance with field work, and reviewers C. Kilburn, H. Pinkerton, and G. Walker for their helpful comments.

References

Bagdassarov NS, Dingwell DB (1992) A rheological investigation of vesicular rhyolite. J Volcanol Geotherm Res 50: 307–322

Baloga SM, Glaze LS, Crisp JA, Stockman SA (1998) New statistics for estimating the bulk rheology of active lava flows: Puʻu ʻŌʻō examples. J Geophys Res 103: 5133–5142

Barnard WM (1990) Mauna Loa: a source book. Historical eruptions and exploration, vol 1: from 1778 Through 1907. Suny Fredonia, Fredonia, New York, pp 1–353

Bentley BJ, Leal LG (1986) An experimental investigation of drop deformation and breakup in steady, two-dimensional linear flows. J Fluid Mech 167: 241–283

Cashman KV (1993) Relationship between crystallization and cooling rate-insight from textural studies of dikes. Contrib Mineral Petrol 113: 126–142

Cashman KV, Kauahikaua JP (1997) Reevaluation of vesicle distributions in basaltic lava flows. Geology 25: 419–422

Cashman KV, Mangan MT, Newmann S (1994) Surface degassing and modifications to vesicle size distributions in active basalt flows. J Volcanol Geotherm Res 61: 45–68

Cashman KV, Kauahikaua JP, Thornber C (1997) Cooling and crystallization in open lava channels (Abstract). EOS Trans AGU 78: F793

Chester DK, Duncan AM, Guest JE, Kilburn CRJ (1985) Mount Etna: the anatomy of a volcano. Chapman and Hall, London, pp 1–300

Crisp JA, Baloga SM (1990) A model for lava flows with two thermal components. J Geophys Res 95: 1255–1270

Crisp JA, Baloga SM (1994) Influence of crystallization and entrainment of cooler material on the emplacement of basaltic ʻaʻā flows. J Geophys Res 99: 11819–11831

Crisp J, Cashman KV, Bonini JA, Hougen SB, Pieri DC (1994) Crystallization history of the 1984 Mauna Loa lava flow. J Geophys Res 99: 7177–7198

Dingwell DB, Webb SL (1989) Structural relaxation in silicate melts and non-Newtonian melt rheology in geologic processes. Phys Chem Mineral 16: 508–516

Dragoni M (1993) Modelling the rheology and cooling of lava flows. In: Kilburn CRJ, Luongo G (eds) Active lava flows: monitoring and modelling. UCL Press, London, pp 235–261

Fink JH, Griffiths RW (1990) Radial spreading of viscous-gravity currents with solidifying crust. J Fluid Mech 221: 485–509

Gaonac'h H, Stix J, Lovejoy S (1996) Scaling effects on vesicle shape, size and heterogeneity of lavas from Mount Etna 74: 131–153

Gay EC, Nelson PA, Armstrong KP (1969) Flow properties of suspensions with high solids concentrations. Am Inst Chem Eng J 15: 815–822

Gregg TKP, Fink JH (1995) Quantification of submarine lava-flow morphology through analog experiments. Geology 23: 73–76

Griffiths RW, Fink JH (1992a) Solidification and morphology of submarine lavas: a dependence on extrusion rate. J Geophys Res 97: 19729–19737

Griffiths RW, Fink JH (1992b) The morphology of lava flows in planetary environments: predictions from analog experiments. J Geophys Res 97: 19739–19748

Griffiths RW, Fink JH (1993) Effects of surface cooling on the spreading of lava flows and domes. J Fluid Mech 252: 667–702

Head JW, Wilson L (1987) Lava fountain heights at Puʻu ʻŌʻo, Kilauea, Hawaiʻi: indicators of amount and variations of exsolved magma volatiles. J Geophys Res 92: 13715–13719

Herd RA, Pinkerton H (1997) Bubble coalescence in basaltic lava: its impaction on the evolution of bubble populations. J Volcanol Geotherm Res 75: 137–157

Hon K, Kauahikaua JP, Denlinger R, MacKay K (1994) Emplacement and inflation of Pāhoehoe sheet flows: observations and measurements of active lava flows on Kilauea Volcano, Hawaiʻi. Geol Soc Am Bull 106: 351–370

Keszthelyi L (1994) Calculated effects of vesicles on the thermal properties of cooling basaltic lava flows. J Volcanol Geotherm Res 63: 257–266

Keszthelyi L (1995) A preliminary thermal budget for lava tubes on the Earth and planets. J Geophys Res 100: 20411–20420

Keszthelyi L, Denlinger R (1996) The initial cooling of pāhoehoe flow lobes. J Volcanol Geotherm Res 58: 5–18

Kilburn CRJ (1981) Pāhoehoe and ʻaʻā lavas: a discussion and continuation of the model by Peterson and Tilling. J Volcanol Geotherm Res 11: 373–389

Kilburn CRJ (1990) Surfaces of ʻaʻā flow fields on Mount Etna, Sicily: morphology, rheology, crystallization and scaling phenomena. In: Fink JH (ed) Lava flows and domes: emplacement mechanism and hazard implications. Springer, Berlin Heidelberg New York, pp 129–156

Kilburn CRJ (1993) Lava crust, Aa flow lengthening and the pāhoehoe–ʻaʻā transition. In: Kilburn CRJ, Luongo G (eds) Active lava flows: monitoring and modelling. UCL Press, London, pp 263–280

Kilburn CRJ, Guest JE (1993) Aa lavas of Mount Etna, Sicily. In: Kilburn CRJ, Luongo G (eds) Active lava flows: monitoring and modelling. UCL Press, London, pp 73–106

Kouchi A, Tsuchiyama A, Sunagawa I (1986) Effects of stirring on crystallisation kinetics of basalt: texture and element partitioning. Contrib Mineral Petrol 93: 429–438

Lesher CE, Cashman KV, Mayfield JD (in press) Kinetics controls on crystallization of Tertiary North Atlantic basalt and implications for the emplacement and cooling histories of lava at Site 989, SE Greenland rifted margin. Proc ODP Sci Results Leg 163

Lipman PW, Banks NG (1987) Aa flow dynamics, Mauna Loa, 1984. US Geol Surv Prof Pap 1350: 1527–1567

Lipman PW, Banks NG, Rhodes JM (1985) Degassing-induced crystallization of basaltic magma and effects on lava rheology. Nature 317: 604–607

Lockwood JP, Lipman PW (1987) Holocene eruptive history of Mauna Loa Volcano. US Geol Surv Prof Pap 1350: 509–535

Macdonald GA (1953) Pāhoehoe, aa and block lava. Am J Sci 251: 169–191

Macdonald GA (1967) Forms and structure of extrusive basaltic rocks. In: Poldervaart AA, Hess HH (eds) Basalt. The Poldervaart treatise on Rocks of Basaltic Composition, vol 1. Wiley, New York, pp 1–61

Macdonald GA (1972) Volcanoes. Prentice-Hall, Englewood Cliffs, New Jersey, pp 1–501

Manga M, Stone HA (1994) Interactions between bubbles in magmas and lavas: effects of bubble deformation. J Volcanol Geotherm Res 63: 267–279

Manga M, Castro J, Cashman KV, Lowemberg M (1998) Rheology of bubble-bearing magmas. J Volcanol Geotherm Res 87: 15–28

Mangan MT, Cashman KV, Newmann S (1993) Vesiculation of basaltic magma during eruption. Geology 21: 157–160

Marsh BD (1981) On the crystallinity, probability of occurrence and rheology of lava and magma. Contrib Mineral Petrol 78: 85–98

McMillan K, Cross RW, Long PE (1987) Two-stage vesiculation in the Cohasset flow of the Grande Ronde basalt, south-central Washington. Geology 15: 809–812

Montierth C, Johnston DA, Cashman KV (1995) An empirical glass-composition-based geothermometer for Mauna Loa lavas. In: Rhodes JM, Lockwood JP (eds) Mauna Loa revealed. Structure, composition, history and hazards. AGU Books Board, Washington DC, pp 207–217

Moore HJ (1987) Preliminary estimates of the rheological properties of 1984 Mauna Loa lava. In: Decker RW, Wright TL, Stauffer PH (eds) Hawaiian volcanism. US Geol Surv Prof Pap 1350: 1569–1588

Parfitt EA, Wilson L (1995) Explosive volcanic eruptions-IX. The transition between Hawaiian style lava fountaining and Strombolian explosive activity. Geophys J Int 121: 226–232

Peterson DW, Tilling RI (1980) Transition of basaltic lava from pāhoehoe to aa, Kilauea Volcano, Hawai'i: field observations and key factors. J. Volcanol Geotherm Res 7: 271–293

Pinkerton H, Norton GE (1995) Rheological properties of basaltic lavas at sub-liquidus temperatures: laboratory and field measurements on lavas from Mount Etna. J Volcanol Geotherm Res 68: 307–323

Pinkerton H, Sparks RSJ (1976) The 1975 sub-terminal lavas, Mount Etna: a case history of the formation of a compound lava field. J Volcanol Geotherm Res 1: 167–182

Pinkerton H, Sparks RSJ (1978) Field measurements of the rheology of lava. Nature 276: 383–385

Pinkerton H, Stevenson R (1992) Methods of determining the rheological properties of magmas at sub-liquidus temperatures. J Volcanol Geotherm Res 53: 47–66

Pinkerton H, Wilson L (1994) Factors controlling the lengths of channel-fed lava flows. Bull Volcanol 56: 108–120

Pinkerton H, Wilson L (1996) Lava flows on carbonatite and basalt lava flows: similarities, differences and implications for lava flow modelling. In: Whitehead PW (ed) Long lava flows: conference abstracts. James Cook University of North Queensland, Australia pp 48–49

Pinkerton H, Norton GE, Dawson JB, Pyle D (1994) Field observations and measurements of the physical properties of Oldoinyo Lengai alkali carbonatite lavas, November 1988. In: Bell K, Keller J (eds) Carbonatite volcanism of Oldoinyo Lengai: petrogenesis of natrocarbonatite. Springer, Berlin Heidelberg New York, pp 23–36

Polacci M, Papale P (1997) The evolution of lava flows from ephemeral vents at Mount Etna: insights from vesicle distribution and morphological studies. J Volcanol Geotherm Res 76: 1–17

Rhodes JM (1995) The 1852 and 1868 Mauna Loa picritic eruptions: clues to parental magma compositions and the magmatic plumbing system. Geophys Monogr 92: 241–262

Rowland SK, Walker GPL (1987) Toothpaste lava: characteristics and origin of a lava structural type transitional between pāhoehoe and 'a'ā. Bull Volcanol 52: 631–641

Rowland SK, Walker GPL (1990) pāhoehoe and 'a'ā in Hawai'i: volumetric flow rate controls the lava structure. Bull Volcanol 52: 615–628

Russ JC (1986) Practical stereology. Plenum Press, New York, pp 1–185

Ryerson FJ, Weed HC, Piwinski AJ (1988) Rheology of subliquidus magmas. I. Picritic compositions. J Geophys Res 93: 3421–3436

Saar M, Manga M (1999) Permeability parasity relationship in vesicular basalt. Geophys Res Lett 26: 111–114

Sato H (1995) Textural difference between pāhoehoe and aa lavas of Izu-Oshima Volcano, Japan, and experimental study on population density of plagioclase. J Volcanol Geotherm Res 66: 101–113

Shaw HR (1969) Rheology of basalt in the melting range. J Petrol 10: 510–535

Sparks RSJ, Pinkerton H (1978) The effect of degassing on the rheology of basaltic lava. Nature 276: 385–386

Spera FJ, Borgia A, Strimple J, Feigenson M (1988) Rheology of melts and magmatic suspensions. I. Design and calibration of a concentric cylinder viscometer with application to rhyolitic magma. J Geophys Res 93: 10273–10294

Stein DJ, Spera FJ (1992) Rheology and microstructure of magmatic emulsions: theory and experiments. J Volcanol Geotherm Res 49: 57–174

Stone HA (1994) Dynamics of drop deformation and breakup in viscous fluids. Ann Rev Fluid Mech 26: 65–102

Taylor GI (1934) The formation of emulsions in definable fields of flow. Proc R Soc Lond Ser A 146: 501–523

Thornber CR, Heliker CC, Reynolds JR, Kauahikaua JP, Okubo P, Lisowski M, Sutton J, Clague D (1996) The eruptive surge of February 1, 1996: a highlight of Kilauea ongoing east rift zone eruption (abs). EOS Trans AGU 77: F798

Walker D, Powell MA, Logfren GE, Hays JF (1978) Dynamic crystallization of a eucritic basalt. Proc Ninth Lunar Planet Sci Conf, pp 1369–1391

Walker GPL (1989) Spongy pāhoehoe in Hawai'i: a study of vesicle distribution patterns in basalt and their significance. Bull Volcanol 51: 199–209

Webb SL, Dingwell DB (1990) Non-Newtonian rheology of igneous melts at high stresses and strain rates: experimental results from rhyolite, andesite, basalt and nephelinite. J Geophys Res 95: 15695–15701

Wilmoth RA, Walker GPL (1993) P-type and S-type pāhoehoe: a study of vesicle distribution patterns in Hawaiian lava flows. J Volcanol Geotherm Res 55: 129–142

Wilson L, Head JW (1981) Ascent and eruption of basaltic magma on the earth and moon. J Geophys Res 86: 2971–3001